TÜBİTAK

Research Article

Multidirectional power flow in three-port isolated DC-DC converter for multiple battery stacks

Chandra Sekhar NALAMATI*◉**, Niranjan KUMAR**◉**, Rajesh GUPTA**◉

Department of Electrical Engineering, Faculty of Engineering
Motilal Nehru National Institute of Technology Allahabad, India

Abstract: The advances in the field of power electronics have created a superior platform for interfacing clean renewable resources with the ever-growing energy storage technology. In this paper, a multidirectional power flow operation in the three-port isolated DC-DC converter (TBDC) topology has been demonstrated for interfacing different battery energy storage sections to increase the system reliability. Comparison of multiple battery integration with dual active bridge and TBDC has been presented. Converter analysis has been conducted using the Fourier series harmonic model and converter loss calculation is also presented. Power flow controller has been proposed for closed-loop control of the TBDC. The performance of the converter has been tested using MATLAB-based simulation and three modes of power flow control operation have been verified through scaled down laboratory experimental setup.

Key words: Multiport converter, bidirectional isolated DC-DC converter, electrical energy storage

1. Introduction

The increasing demand of energy cannot be met alone by conventional energy sources as they are limited and exhaustible. To meet this increasing demand of energy from renewable sources require integration with the system and storage. Energy from renewable sources is not always available; thus, electrical battery storage section integration is desired to store excess power available in the system during low load demand and to support the deficit power in need of high demand [1, 2]. Bidirectional DC-DC converter ensures an efficient way of fetching deficit power or storing the excess power in the available storage system. Bidirectional converters are of nonisolated and isolated types. For low and medium power scenarios, DC-DC converter without galvanic isolation are used and for large power scenarios, isolated converters are suitable. A DC-DC converter configuration possessing galvanic isolation allows flexibility for overcoming limitations such as voltage mismatch and for safety. Dual active bridges (DAB) are extensively used converters among different galvanically isolated DC-DC bidirectional converters which can accommodate only one battery section [3–5].

For medium and high power application and to integrate more battery sections, DC-DC converter with large rated power electronic devices and modular DC-DC converters with low rated power electronic devices can be used. The former solution is not feasible, whereas modular DC-DC converters can use either converter level modularity (DAB-based) or cell level modularity. In the single-stage two-port DC-DC converters scenario, the growing number of sources and loads results in increased need of DC-DC converter sections to accommodate them into the system and to exchange the power. Effective utilization of renewable energy sources with improved

---

*Correspondence: chandu3072002@gmail.com

reliability can be accomplished with integration of multiple energy sources and electrical energy storage stacks through an efficient single-stage multiport power electronics DC-DC converters [6–8]. Such converters help in reduction of overall energy conversion system size and corresponding controllers needed [9].

Various multiple active bridge (MAB) topologies based on converter modularization and cell level modularization have been reported in the literature [10–20]. The topology of three-port isolated bidirectional DC-DC converter (TBDC) is a member of the MAB family. The cell level modularization configuration (TBDC) uses a multiport converter with multiwinding isolated high-frequency transformer to enable galvanic isolation and matching of voltages among the converter three ports as well as to control multidirectional power flow capability with phase shift control techniques [10–14]. In the literature, various DAB power flow control techniques providing phase-shift control (single phase shift) and duty-cycle control with phase-shift control (dual phase shift, extended phase shift and triple phase shift) that can also be applicable to TBDC topology have been discussed [15, 16]. Among the four control methods mentioned above, single phase-shift control (with fixed duty ratio) has features such as global maximum power transfer, ease of implementation, and simple bidirectional power flow control compared to the other three methods. With increased implementation complexity, other three methods can improve wide range power control. In the literature, the TBDC topology has been explained and analysis has also been reported [17–20].

In this paper, the operation of TBDC topology has been discussed for multiple battery stack applications with all possible modes of power transfer. Analysis using the Fourier series harmonic model has been done and converter loss calculation has been discussed. Closed-loop control of the TBDC has been presented. Comparison of multiple battery integration with DAB and TBDC has been presented. Converter multidirectional power flow transfer capability through three modes of operation with the help of simulation as well as laboratory experimental set up has been demonstrated.

Section 2 provides a detailed description of the TBDC. Section 3 describes the TBDC analysis, loss model, and its control strategy. Section 4 presents a detailed comparison of modular and cell level modularization. Section 5 presents the test results and discussion of TBDC using MATLAB software. Performance of the TBDC has been verified in different modes of operation with the help of experimental results in Section **??**.

2. Description of three-port bidirectional DC-DC converter

Figure 1 depicts a detailed block diagram of the multiple battery sections integrated TBDC for large electrical energy storage applications. The TBDC consists of a high-frequency multiwinding transformer having one high voltage side and two secondary windings and also one H-bridge on high-voltage (HV) and two low-voltage (LV) H-bridges. Each bridge has four high-frequency operated switches. High-frequency transformers have the advantage of reduced size for the same power transfer compared with the normal low-frequency bulky transformers. The multiwinding isolated high-frequency transformer enables galvanic isolation and matching of voltages among the power-electronic-switch–based converter three ports. The DC-link can be formed from the DC-micro grid having various renewable energy sources and it supplies power to the TBDC, whereas battery-based electrical energy storage sections are integrated with the LV inverter bridges of the TBDC. The TBDC has the bidirectional power flow capability. Power flow among the three transformer ports has been controlled by controlling the phase-shift angle between HV and LV high-frequency AC voltages produced at transformer ports. Two inductors are connected to low-voltage inverter bridge to create the phase shift; thus, two phase shift angles are generated with respect to HV bridge output. In the TBDC power flow control, one side bridge voltage output waveform (V_{HV}) helps as a reference for generation of the control signals for the other two LV

side inverter voltage waveforms (V_{LV1} and V_{LV2}). The angles of the phase shift ϕ_1 and ϕ_2 generated by the TBDC power flow controller enable smooth power transfer among the HV and two battery sections (battery 1 and 2). The phase shifts ϕ_1 and ϕ_2 controls the power in TBDC from $\pi/2$ to $\pi/2$ as control range. On the basis of phase-shift angles, different modes of operation of TBDC have been described. There are three modes of operation in Figure 2 as discussed below:
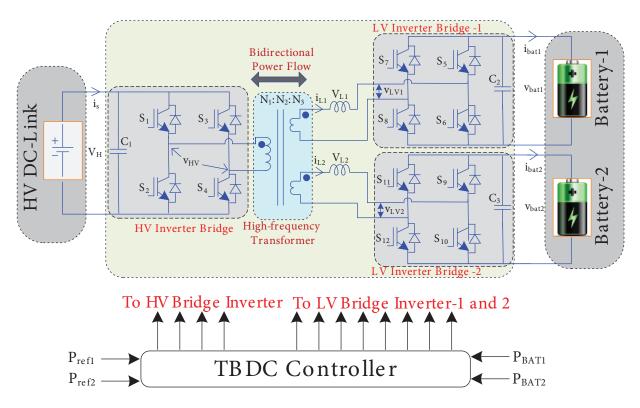

Figure 1. Detailed circuit diagram of multiple battery sections integrated three-port bidirectional DC-DC converter.

(a) $\phi_1 > 0°$ and $\phi_2 > 0°$: This mode of operation takes place in the system when there exists excess generated power with the microgrid after fulfilling the load demand. Figure 2a depicts the waveforms of voltage and inductor current at transformer ports and corresponding power flow diagram for this mode. The duty ratio of the voltage waveform across HV side and LV sides is considered as 0.5 with fixed pulse width modulation. Phase-shift angles ϕ_1 and ϕ_2 are lagging with respect to the HV bridge waveform; hence, power transfers to LV sides (batteries) from the HV side and both batteries are charging from the power supplied from HV source. The batteries installed at LV sides can have different ratings. The phase angle magnitude confirms the amount of power to be transferred to the batteries. For example, if $0° < \phi_2 < \phi_1 < 90°$ then power transferred from the source to battery 1 is more than the power transferred to battery 2.

(b) $\phi_1 < 0°$ and $\phi_2 < 0°$: This mode occurs in the system when there exists excess load demand higher than the available generation from the energy sources. The voltage and inductor current waveforms and corresponding power flow diagram for this mode is depicted in Figure 2b. Phase-shift angles ϕ_1 and ϕ_2 of TBDC are leading with reference to the HV bridge waveform, which results in transfer of power from the two batteries of storage section to the DC-link through the HV bridge. The phase angle magnitude decides the amount of power to be transferred to the HV side from the battery section. For example, if $-90° < \phi_1 < \phi_2 < 0°$ then
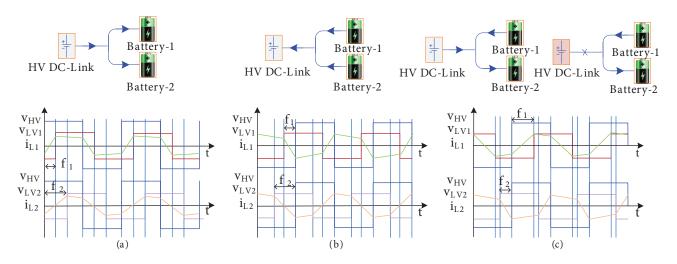
Figure 2. Voltage and current waveforms of TBDC (a) $\phi_1 > 0°$ and $\phi_2 > 0°$, (b) $\phi_1 < 0°$ and $\phi_2 < 0°$, and (c) $\phi_1 > 0°$ and $\phi_2 < 0°$.

power transferred from battery 1 to source is more than the power transferred from battery 2.

(c) $\phi_1 > 0°$ and $\phi_2 < 0°$: Figure 2c shows the voltage and current waveforms at transformer ports and power flow diagram for this mode. In this mode ϕ_1 is lagging and ϕ_2 is leading with respect to HV bridge voltage waveform. Voltage waveform of one LV bridge is lagging with respect to HV bridge, whereas waveform of another bridge is leading with respect to HV bridge. This mode is possible when battery 2 demands more power than the available generation in the system and is not capable to supply the power. The power deficit will be supplied by battery 1; hence, power will flow from source and battery 1 to battery 2. In another special case, when power from renewable sources is not available due to their intermittent nature, power from HV side is not available. In such scenario, battery 1 alone supplies the required power to battery 2, which highlights power exchanged between energy storage devices when the source is not available. In the case where one of the variables of TBDC, either ϕ_1 or ϕ_2, is zero, operation of TBDC will resemble the operation of a conventional DAB. The facility to integrate multiple battery storage stacks through the two available output ports yields the advantage of increased reliability.

3. Analysis and control strategy of TBDC

3.1. Analysis of TBDC

The steady-state analysis of the TBDC with single phase-shift control method has been carried out using DAB converter analysis by considering ideal components [20]. Here $V'_{HV}(=V_{HV}/n)$, V_{LV1}, and V_{LV2} are square waveforms with 0.5 duty ratio. V_H is the HV side volatge, V_{bat1} and V_{bat2} are the battery voltages, ω is switching angular frequency, and L_{xy} (x,y:1,2,3) represents equivalent winding inductance of port x and y. Power flows from inverter waveform with leading voltage side to lagging voltage port, depending on the two ends of the inductors connected to each LV inverter bridge. TBDC topology can be represented in a delta-connected or star-connected fashion for analysis purposes as shown in Figure 3. In this paper, analysis has been carried out from the delta-connected equivalent circuit by considering large transformer magnetizing inductance in comparison with equivalent inductances of Figure 1. $V'_{HV}(=V_{HV}/n)$ will act as a reference, V_{LV1n} and V_{LV2n} are phase-shifted by phase-shift angles ϕ_1 and ϕ_2. The square wave voltages of the three ports of the converter
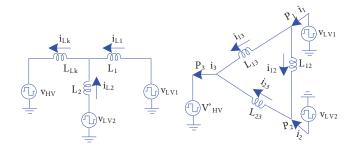
can be represented by the Fourier series as below (1)–(3):

Figure 3. TBDC equivalent circuits

$$v_{LV1}(t) = \frac{4}{\pi} \sum_{n=1,3,5..}^{\infty} \frac{1}{n}[V_{bat1} \sin n(\omega t + \phi_1)] \tag{1}$$

$$v_{LV2}(t) = \frac{4}{\pi} \sum_{n=1,3,5..}^{\infty} \frac{1}{n}[V_{bat2} \sin n(\omega t + \phi_2)] \tag{2}$$

$$v_{HV}'(t) = \frac{4}{\pi} \sum_{n=1,3,5..}^{\infty} \frac{1}{n}[V_H \sin n(\omega t)] \tag{3}$$

The above Fourier series-based voltages (1)–(3) of TBDC can be represented in the phasor form for simplification as (4).

$$\left. \begin{aligned} \mathbf{V}_{LV1n} &= V_{LV1n}\angle n\phi_1 \\ \mathbf{V}_{LV2n} &= V_{LV2n}\angle n\phi_2 \\ \mathbf{V}_{HVn}' &= V_{HVn}\angle 0 \end{aligned} \right\} \tag{4}$$

Here V_{LV1n}, V_{LV2n} and V_{HV}' $(=V_{HV}/n)$ represents the root mean square value (RMS) of the nth harmonic voltage component. The harmonic current phasors have been calculated from the phasor harmonic voltages and the corresponding inductances as (5). I_{xyn} (x,y:1,2,3) represents the current flowing from port x to port y. The currents flowing through the different TBDC ports (5) can also be represented using voltage phasors (6) and in terms of real and imaginary parts as depicted in (7).

$$\left. \begin{aligned} I_{12n} = -I_{21n} &= \frac{1}{n\omega L_{12}}(V_{LV1n}\angle n\phi_1 - V_{LV2n}\angle n\phi_2) \\ I_{13n} = -I_{31n} &= \frac{1}{n\omega L_{13}}(V_{LV1n}\angle n\phi_1 - V_{HVn}\angle 0) \\ I_{23n} = -I_{32n} &= \frac{1}{n\omega L_{23}}(V_{LV2n}\angle n\phi_2 - V_{HVn}\angle 0) \end{aligned} \right\} \tag{5}$$

$$I_{12n} = \frac{1}{n\omega L_{12}}\left[V_{LV1n}(\sin n\phi_1 - i\cos n\phi_1) - V_{LV2n}(\sin n\phi_2 - i\cos n\phi_2)\right]$$

$$I_{13n} = \frac{1}{n\omega L_{13}}\left[V_{LV1n}(\sin n\phi_1 - i\cos n\phi_1) + i\, V_{HVn}\right] \qquad (6)$$

$$I_{23n} = \frac{1}{n\omega L_{23}}\left[V_{LV2n}(\sin n\phi_2 - i\cos n\phi_2) + i\, V_{HVn}\right]$$

$$I_{1n} = I_{12n} + I_{13n} = A_{1n} + iB_{1n}$$
$$I_{2n} = I_{23n} + I_{21n} = A_{2n} + iB_{2n} \qquad (7)$$
$$I_{3n} = I_{31n} + I_{32n} = A_{3n} + iB_{3n}$$

The power transfer between any two ports of the TBDC topology has been derived in (8) using the voltage and current expressions defined above (1)–(7). P_{xy} (x,y:1,2,3) represents the power flow from port x to port y.

$$P_{12} = -P_{21} = \sum_{n=1,3,5..}^{\infty} \frac{1}{n\omega L_{12}}\left[V_{LV1}V_{LV2}\sin n\phi_{12}\right]$$

$$P_{13} = -P_{31} = \sum_{n=1,3,5..}^{\infty} \frac{1}{n\omega L_{13}}\left[V_{LV1}V_{HV}\sin n\phi_{13}\right] \qquad (8)$$

$$P_{23} = -P_{32} = \sum_{n=1,3,5..}^{\infty} \frac{1}{n\omega L_{23}}\left[V_{LV2}V_{HV}\sin n\phi_{23}\right]$$

The expressions (P_1, P_2, P_3) in (9) describe the active power transfer capability of the TBDC topology with the square wave modulation from the one port to the other two ports through the high-frequency transformer AC-link.

$$P_1 = P_{12} + P_{13}$$
$$P_2 = P_{23} + P_{21} \qquad (9)$$
$$P_3 = P_{31} + P_{32}$$

Total power flowing through the converter should be balanced in each mode as discussed in the above section and the same can be understood by equation (9).

3.2. TBDC loss model

The performance of the TBDC can be understood by calculating the losses incurred in the system as defined in (10) below. The total losses can be classified into losses in the power semiconductor devices (P_{sc}), losses in high-frequency transformer AC-link (P_{tx}), and losses due to the passive component ($P_{passive}$) in the TBDC converter system.

$$P_{Losses} = P_{sc} + P_{tx} + P_{passive} \qquad (10)$$

The losses in the AC-link high-frequency transformer (P_{tx}) can be divided into iron loss (P_{CL}) and copper loss (P_{CoreL}). The operating frequency of the TBDC converter and core material chosen for the converter magnetic

will decide the iron loss. In this paper, ferrite core with litz wire, $220 mm^2$ core area, 20 turns on primary, 10 turns on the two secondary windings and switching frequency 25 kHz has been considered for transformer design. The copper loss can be calculated using the RMS values of the currents. Expressions defined in (7) can be derived in (11), where (R_{1n}), (R_{2n}), and (R_{3n}) are the transformer AC-resistances.

$$P_{CL} = I_{1n}^2 R_{1n} + I_{2n}^2 R_{2n} + I_{3n}^2 R_{3n} \qquad (11)$$

The familiar Steinmetz equation has been used to calculate the transformer core loss [11, 20], which depends on the waveform of the voltage, operating frequency, core area, and the magnetic flux defined in (12) below.

$$P_{CoreL} = kf^m * 10^m * V_{rms} \frac{1}{4.44 * N * f * Ae} \qquad (12)$$

Switching loss and conduction loss together are combined in losses in the power semi conductor devices(Psc). The conduction losses of the switching devices can be calculated using the RMS values of the currents expressions derived in (7) and channel resistance of the switching devices obtained in (13) below.

$$P_{CondL} = 4 * R_{ds} * (I_{1n}^2 + I_{2n}^2 + I_{3n}^2) \qquad (13)$$

The on and off switching intervals and the switching frequency, drain voltage, and currents are responsible for the switching losses [10, 11]. The losses due to the passive components ($P_{passive}$) such as inductor and capacitor can be calculated by measuring the resistances and RMS currents of the inductor and capacitors. For the high-frequency operation, ferrite core with litz wire has been used for inductor design. In TBDC topology, the total losses calculated are less than 10% of the total converter power.

3.3. Control strategy

Effective power flow management in the TBDC having three different ports with single phase-shift control method is achieved using an efficient control strategy which controls the power flow via TBDC as shown in Figure 4. The power flow controller controls the average charging or discharging current of each battery by nearly maintaining battery voltage as constant with the help of phase-shift control. In bidirectional converters, the duty ratio helps to control the battery current. The power flow controller determines the required step change in the duty ratio after comparing actual and reference battery powers, which results in either increment or decrement of the present duty ratio. Correspondingly, the battery may operate in charging or discharging mode.

The battery power (P_{bat1} and P_{bat2}) has been determined instantaneously by sensing the actual battery voltage and currents and compared with the reference battery power (P_{ref1} and P_{ref2}). Then the phase angle shifts (ϕ_1 and ϕ_2) have been determined after passing the resultant power difference through the PI controller and limiter section. Appropriate values of K_P and K_I have been chosen to get the required phase-shift angle. Furthermore, the phase-shift angles are converted into the time delay and provided as input to the time delay block. The resultant control signal has been phase-shifted with respect to the reference pulse (lagging or leading) that determines the TBDC operation in forward or reverse mode. The square wave gate pulses with 50% duty cycle are used as triggering pulses for TBDC power semiconductor switches S_1 & S_4 in the HV inverter and they are generated by comparing a triangular wave with the modulating signal as shown in Figure 4. They act as a reference pulse for generating control signals for the switches S_2 and S_3 of HV bridge and also for both
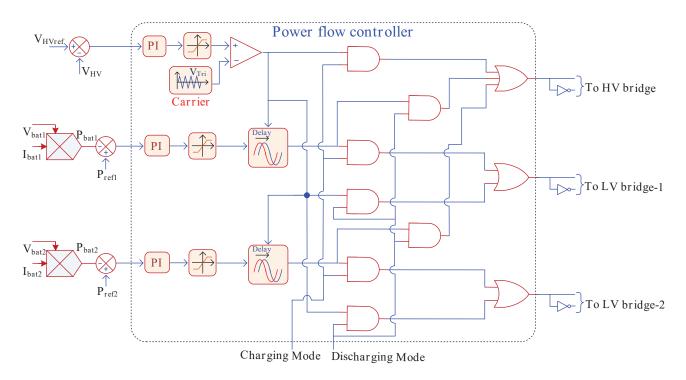
Figure 4. TBDC controller for gate pulse generation.

LV inverter bridge switches in the transformer secondary. The digital section in the power flow controller helps in directing the correct switching signals to the power electronic switches. It interchanges the control pulses in each corresponding mode of operation (charging to discharging and vice versa).

4. Comparison of multiple battery integration with DAB modular converter and TBDC

Efficient DC-DC converter topologies help to fulfill the requirements of high power applications with bidirectional power flow capability and isolation. For this, DC-DC converters having large rating power electronic devices and modular DC-DC converters with low rating power electronic devices can be used. The former solution is not feasible, whereas modular DC-DC converters can use either converter level modularity or cell level modularity. Multiple battery integration using multiple DAB converters is recognized as the converter modularization (conventional system) Figure 5a, whereas multiple battery integration using multiple converter cells (TBDC or the integrated system) topologies have been recognized as the cell level modularization Figure 5b [10, 11]. The latter converter configuration (TBDC) uses multiwinding transformer along with the transformer inductances (leakage and/or external inductances) to couple and transfer the power among the input and output ports and it has advantages such as reduction in the number of power converter cells and the converter volume and it is economical compared to the modular converter discussed above. The concept of multiport DAB can be extended for multiple direction DC-DC converters having more than three-ports. In case of two output ports with the same voltage and the same parameter as DAB, TBDC transfers 33.28% more power than DAB [20]. The placement of the coupling inductors in TBDC also affects its performance and it has been suggested in the literature [19] that impedance of the output bridge should be larger than that of transformer primary. It has also been suggested that placing external inductors on secondary side yields a better performance than placing

on all ports or on the primary alone. The first configuration requires small phase shifts to maintain the two output ports at equal voltages if one port voltage changes due to the variation of the other port voltage [19, 20].
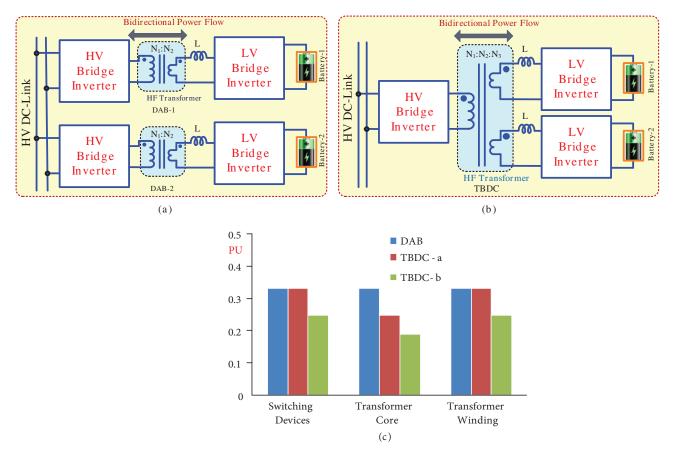

Figure 5. Topologies (a) DAB (b) TBDC (c) cost analysis.

(a) In TBDC/integrated system topology, to integrate two energy storage sections, a single multiwinding transformer (reduction in the number of transformer cores) is required, whereas two individual transformers are required in the DAB converter scenario/conventional system.

(b) TBDC topology requires 4 power electronic semiconductor devices in primary side, whereas conventional system utilizes 8 switching devices.

(c) The two comparisons above indicate reduction of hardware requirement in TBDC topology.

(d) Requirement of magnetics: Reduction in the core mean length in TBDC toplogy results in core volume reduction and correspondingly core cost reduction by one-fourth times compared to the conventional system (14). TBDC, on the other hand, requires large primary winding conductor size which almost compensates for its one primary winding advantage.

$$\left. \begin{aligned} V_{DAB} &= A_e l_{AV} \\ V_{TBDC} &= A_e \frac{3}{4} l_{AV} \end{aligned} \right\} \tag{14}$$

(e) Overall cost analysis Figure 5c

Scenario-1: Both systems with equal power transfer capability in primary section. In TBDC (TBDC-a), 25% cost reduction in magnetic core occurs, whereas costs of the switch and copper winding are equal (as discussed above) [19, 20].

Scenario-2: Power transfer capability of TBDC primary is equal to that of one primary bridge in the conventional system. In this case TBDC (TBDC-b) yields more cost (overall about 33%) reductions in switching devices, transformer core, as well as transformer winding, compared to the conventional system.

5. Simulation results

The simulation of TBDC with single phase-shift control method has been performed on MATLAB r2017a. Figures 6 and 7 depict the SIMULINK results obtained and the model developed in MATLAB software with the help of subblocks, respectively. For the simulation purpose, the parasitics of all the MOSFETs used in the TBDC have been considered, and corresponding input and output powers have been obtained. It is observed that additional power inputs are required to meet the excess losses due to these parasitics. The three modes of operation of the TBDC are given in detail in Figure 2. In this section, the converter bidirectional power flow with the closed loop control using the power flow controller discussed in Section 4 has been shown.
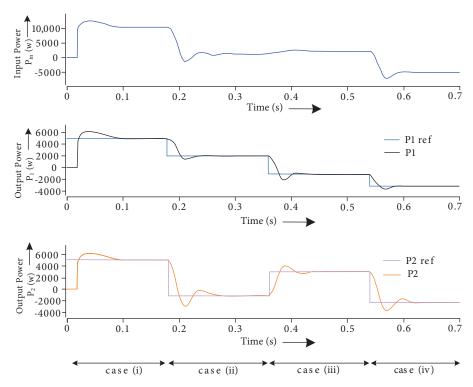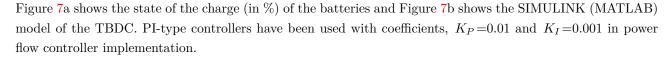

Figure 6. TBDC bidirectional power flow control with different reference powers.

Table 1 shows the simulation parameters of TBDC used in the simulation.

Different values of the power reference have been taken into account to demonstrate the controller performance and operation of the TBDC in terms of power flow. Table 2 shows the values of the power reference in each case, where the negative sign shows the change in power flow direction according to the cases in Table 2. Figure 6 shows the simulation results for the multidirectional power flow capability of the TBDC.
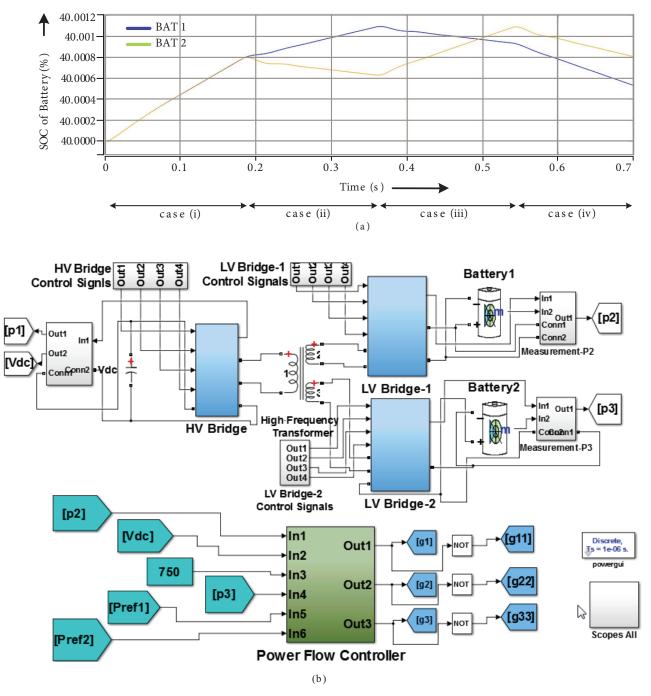
Figure 7a shows the state of the charge (in %) of the batteries and Figure 7b shows the SIMULINK (MATLAB) model of the TBDC. PI-type controllers have been used with coefficients, $K_P=0.01$ and $K_I=0.001$ in power flow controller implementation.

Figure 7. (a) State of charge of batteries (b) Simulink model (MATLAB) of TBDC

Case (i): Figure 6 shows the mode I operation of the TBDC (Figure 2a) as case (i). The battery reference powers are 5 kW each with HV leading LV side scenario. TBDC HV side supplies the required power to the LV

Table 1. Simulation parameters of TBDC.

S. No.	Parameter	Rating
1.	TBDC power rating	11.0 kW
2.	Inductance L_1, L_2	10.0 μH
3.	Converter switching frequency	25.0 kHz
4.	Transformer turns ratio	8:1:1
5.	Nominal voltage of batteries(2 No.)	96.0 V
6.	Voltage at HV port input	750.0 V
7.	Rating of 3-port transformer	25.0 kHz, 15.0 kVA

Table 2. Power references.

Case	Modes of operation	Power references
i.	$\phi_1 > 0° \ \& \ \phi_2 > 0°$	$P_{ref1} = 5$ kW & $P_{ref2} = 5$ kW
ii.	$\phi_1 > 0° \ \& \ \phi_2 < 0°$	$P_{ref1} = 2$ kW & $P_{ref2} = $ -1 kW
iii.	$\phi_1 < 0° \ \& \ \phi_2 > 0°$	$P_{ref1} = $ -1 kW & $P_{ref2} = 3$ kW
iv.	$\phi_1 < 0° \ \& \ \phi_2 < 0°$	$P_{ref1} = $ -3 kW & $P_{ref2} = $ -2 kW

side batteries and, as also seen, equal power transfer to both batteries. Figure 7a shows that both batteries are charging and the amount of power transferred to both batteries is the same; hence, the state of charge is also the same.

Case (ii): Figure 6 shows the mode III operation of the TBDC (Figure 2c). In this case, battery-1 needs 2 kW power which is supported by source and battery 2 which can be observed from Figure 7a, where battery 1 is charging while battery 2 is discharging.

Case (iii): This also shows the mode III operation of TBDC (Figure 2(c)), the required 3 kW power for battery 2 has been supplied by the source and battery 1 (Figure 6). Figure 7a depicts the battery 2 charging and battery 1 discharging with different charge rates. Case (ii) and case (iii) show the possibility of power exchange between two LV sides of TBDC. Approximately 1 kW power has been transferred to battery 1 from battery 2 and to battery 2 from battery 1, in case (ii) and case (iii), respectively.

Case (iv): Figure 6 shows the mode II operation of the TBDC (Figure 2b), i.e. 5 kW power transferred from LV to HV side. Amount of power supplied by each battery is different due to their different reference values. Both batteries are discharging, which can be seen from Figure 7a where their state of charge also decreases. For the controller performance demonstration, all possible modes have been shown in 0.7 s (small duration) with large change in the reference powers (Table 2). Due to this, scenario controller performance parameters such as overshoot and the settling time have been lightly affected.

6. Experimental Results

A scaled-down experimental setup of the TBDC has been developed in the laboratory as shown in Figure 8 to verify the proposed work experimentally. For the simulation studies, the power rating is 11 kW, whereas the experimental work is done at the power rating of 110 W (down-scaled 100 times). Actual results are obtained for 70 W as presented in Figures 9–11. The setup consists of MOSFET (IRF 260N)-based H-bridge inverter

modules, isolated four-channel gate driver boards, ferrite-core-based multiwinding high-frequency transformer and inductors, batteries (4 No. 12V, 7Ah), Arduino UNO microcontroller, voltage and current sensors (LV20P and LA25P), and Tektronix TPS2024 digital storage oscilloscope. Switching frequency of TBDC is 25 kHz. A three-winding high-frequency isolation transformer has one winding on the primary and two windings on the transformer secondary.
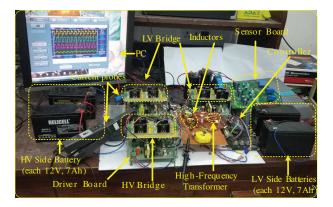

Figure 8. Experimental setup of TBDC.

All three modes of operation have been verified on the laboratory experimental setup of TBDC as depicted in Figure 8. Arduino UNO microcontroller is used to generate the switching pulses at frequency of 25 kHz, these pulses are given as an input to four-channel gate driver boards and output pulses from the gate driver are supplied to the switches. The TBDC has three H-bridge modules; hence, three gate driver boards have been used. All three H-bridges are interconnected through ferrite core multiwinding high-frequency transformer. Each LV inverter bridge has a ferrite core inductor. The parameters for the experimental implementation of the TBDC are given in Table 3.

Table 3. Parameters for experimental setup of TBDC.

1	Transformer turns ratio	2:1:1
2	Transformer operating frequency	25 kHz
3	Inductance (L_1 & L_2)	150 μH
4	Battery	12 V, 7 Ah

6.1. Mode I

Figure 9a depicts the control gating pulses generated from the controller for the switches of the TBDC. On the HV side, 24V DC has been provided by two batteries of 12 V (7 Ah each) and two LV ports are formed by two 12 V (7 Ah each) batteries. The power flow controlled converter phase-shift angles have been chosen as $\phi_1 = 45°$ and $\phi_2 = 80°$ to demonstrate the power flow operation from HV to LV side. Voltage waveforms of HV inverter bridge (V_{HV}), LV inverter bridge 1 (V_{LV1}) and bridge 2 (V_{LV2}), and inductor current waveform of the LV bridge 1 (I_{L1}) are shown in Figure 9b, where V_{HV} is leading both the V_{LV1} and V_{LV2}. Power flow operation can be observed in Figure 9c in terms of the converter currents 2 A, 1.8 A, and 2 A as source current (I_s), battery 1 current (I_{B1}) and battery 2 current (I_{B2}), respectively. HV side converter supplies 48 W of
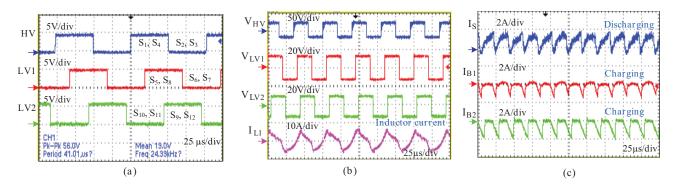
power to two LV batteries.

Figure 9. Operation of TBDC in Mode I: (a) switching pulses, (b) voltage waveforms of HV and LV bridges and inductor current waveforms, (c) current waveforms.

6.2. Mode II

The switching pulses for this mode have been generated and are depicted in Figure 10a. The $\phi_1 = -65°$ and $\phi_2 = -35°$ are converter phase-shift angles where the negative sign indicates that HV bridge output voltage V_{HV} is lagging from both the LV bridge output voltages V_{LV1} and V_{LV2}. Voltage waveforms of HV bridge (V_{HV}), LV bridge 1 (V_{LV1}) and bridge 2 (V_{LV2}), and inductor current waveform of the LV bridge 1 (I_{L1}) are shown in Figure 10b, and observed that V_{HV} is lagging behind both V_{LV1} and V_{LV2}. Power flow operation has been observed from the Figure 9c in terms of the converter currents i.e. source current (I_s), battery 1 current (I_{B1}) and battery 2 current (I_{B2}) of 2 A, 3 A, and 0.8 A, respectively. Power demand of 48 W by the HV side converter has been supported by the two LV batteries with higher power support from battery 1 due to large phase-shift.
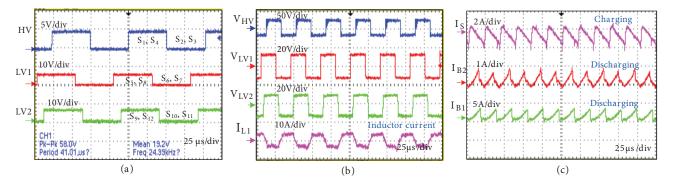

Figure 10. Operation of TBDC in Mode II: (a) switching pulses, (b) voltage waveforms of HV and LV bridges and inductor current waveforms, (c) current waveforms.

6.3. Mode III

The switching pulses for this mode have been generated and are shown in Figure 11a. Phase-shift angles have been chosen as $\phi_1 = -30°$ and $\phi_2 = 75°$ with V_{HV} lagging V_{LV1} and (V_{LV1}) leading (V_{LV2}). Figure 11b depicts the voltagewave forms of primary side HV bridge (V_{HV}), LV bridge 1 (V_{LV1}) and bridge 2 (V_{LV2}), and

inductor current waveform of the LV bridge 1 (I_{L1}). Power flow operation can be observed in Figure 11c in terms of the converter currents 2 A, 5.5 A, and 1 A as source current (I_s), battery 1 current (I_{B1}), and battery 2 current (I_{B2}), respectively. Both the HV side bridge and LV bridge battery 2 have been supplied with 6 5W power by battery 1.
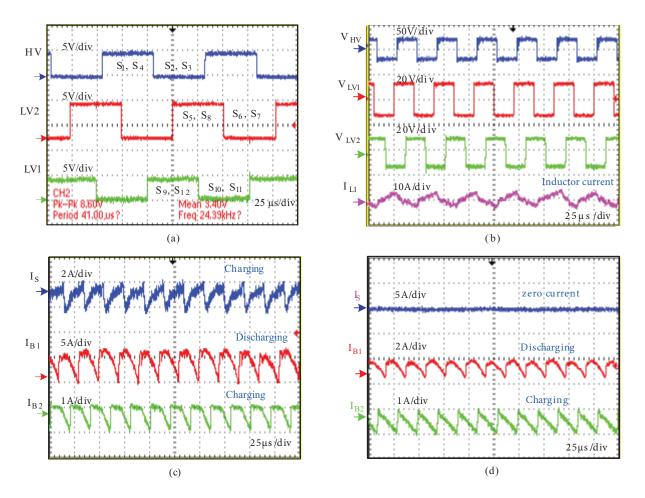

Figure 11. Operation of TBDC in Mode III: (a) switching pulses, (b) voltage waveforms of HV and LV bridges and inductor current waveforms, (c) current waveforms, (d) battery current waveforms when source current is zero.

Figure 11d shows the special case of mode III where only power exchange happens between the LV bridge 1 and bridge 2 in terms of the currents. In this case, source current is zero, which indicates that there has been no power exchange from transformer primary HV side to LV sides. Figure 11d depicts that battery 1 is discharging (1.2 A) and battery 2 is charging (1 A); hence, 14 W power is transferred to battery 2 from battery 1. Total power loss of 70 W associated with the TBDC experimental setup has been calculated. The total efficiency of the system has been found to be more than 90%. MOSFET switch conduction losses and switching losses dominate the total system losses. Losses obtained as MOSFET conduction losses are 2.33 W, switching losses are 1.833 W, transformer losses are 0.5 W, and other losses are less than 0.5 W. System efficiency has been obtained around 93%.

7. Conclusion

In this paper, a three-port isolated multidirectional power flow DC-DC converter topology operation and its analysis based on Fourier series harmonic model for interfacing the multiple battery storage sections has been proposed. The converter operation has been presented in three possible modes and power flow controller has been proposed for reliable multidirectional power transfer. Feasibility of multiple battery sections interfacing with DAB modular converter and TBDC has been presented in detail along with cost savings. The loss calculation has been presented and efficiency has been measured as around 93%. The converter performance has been tested using both the simulation and experimental platforms in three modes of operation and power balancing has been achieved.

Acknowledgment

References

[1] Pazheri F, Othman MF, Malik NH, Al-Arainy AA. Energy-efficient and environmentally friendly power dispatch by trigeneration with renewable energy and energy storage. Turkish Journal of Electrical Engineering & Computer Sciences 2016; 24(6): 5161-5161. doi: 10.3906/elk-1405-95

[2] Paul A, Subramanian K, Nachinarkiniyan S. PV-based off-board electric vehicle battery charger using BIDC. Turkish Journal of Electrical Engineering & Computer Sciences 2019; 27(4): 2850-2865. doi: 10.3906/elk-1804-227

[3] De Doncker RWAA, Divan DM, Kheraluwala MH. A three-phase soft-switched high-power-density dc /dc converter for high-power applications. IEEE Transactions on Industry Applications 1991; 27(1): 63-73. doi: 10.1109/28.67533

[4] Sharma R, Suhag S. Supercapacitor utilization for power smoothening and stability improvement of a hybrid energy system in a weak grid environment. Turkish Journal of Electrical Engineering & Computer Sciences 2018; 26(1): 347-362. doi: 10.3906/elk-1703-101

[5] Bakan AF. A new LVI assisted PSFB DC-DC converter. Turkish Journal of Electrical Engineering & Computer Sciences 2011; 19(2): 191-206. doi: 10.3906/elk-1001-352

[6] Behjati H, Davoudi A. A multiple-input multiple-output DC-DC converter. IEEE Transactions on Industry Applications 2013; 49(3): 1464-1479. doi: 10.1109/TIA.2013.2253440

[7] Sepehr A, Saradarzadeh M, Farhangi S. High-voltage isolated multioutput power supply for multilevel converters. Turkish Journal of Electrical Engineering & Computer Sciences 2017; 25(4): 3319-3333. doi: 10.3906/elk-1604-410

[8] Nalamati CS, Agrawal A, Gupta R. Integration of multiple energy storage sections in solar PV based HMGs using multi-input DAB. In: IEEE 2018 PEDES International Conference on Power Electronics, Drives and Energy Systems; Chennai, India; 2018. pp. 1–6. doi: 10.1109/PEDES.2018.8707522

[9] Ji Z, Sun Y, Jin C, Wang J, Zhao J. A coordinated DC voltage control strategy for cascaded solid state transformer with star configuration. Turkish Journal of Electrical Engineering & Computer Sciences 2019; 27(1): 634-648. doi: 10.3906/elk-1805-183

[10] Rahman M A, Islam MR, Muttaqi KM, Sutanto D. Modeling and control of SiC-based high-frequency magnetic linked converter for next generation solid state transformers. IEEE Transactions on Energy Conversion 2020; 35(1): 549-559. doi: 10.1109/TEC.2019.2940042.

[11] Costa LF, Hoffmann F, Buticchi G, Liserre M. Comparative analysis of multiple active bridge converters configurations in modular smart transformer. IEEE Transactions on Industrial Electronics 2019; 66(1): 191-202. doi: 10.1109/TIE.2018.2818658.

[12] Tao H, Kotsopoulos A, Duarte JL, Hendrix MAM. Triple-half-bridge bidirectional converter controlled by phase shift and PWM. In: IEEE 2006 APEC Twenty-First Annual Applied Power Electronics Conference and Exposition; Dallas, TX, USA; 2006. pp. 1-7. doi: 10.1109/APEC.2006.1620700

[13] Zhao C, Round SD, Kolar JW. An isolated three-port bidirectional dc-dc converter with decoupled power flow management. IEEE Transactions on Power Electronics 2008; 23(5): 2443-2453. doi: 10.1109/TPEL.2008.2002056

[14] Liu R, Xu L, Kang Y, Hui Y, Li Y. Decoupled TAB converter with energy storage system for HVDC power system of more electric aircraft. The Journal of Engineering 2018; 13: 593-602. doi: 10.1049/joe.2018.0033

[15] Zhao B, Song Q, Liu W, Sun Y. Overview of dual-active-bridge isolated bidirectional DC-DC converter for high-frequency-link power-conversion system. IEEE Transactions on Power Electronics 2014; 29(8): 4091-4106. doi: 10.1109/TPEL.2013.2289913

[16] Karthikeyan V, Gupta R. Varying phase angle control in isolated bidirectional DC-DC converter for integrating battery storage and solar PV system in standalone mode. IET Power Electronics 2017; 10(4): 471-479. doi: 10.1049/iet-pel.2016.0162

[17] Kumar N, Agrawal A, Gupta R. Split bridge bi-directional DAB converter for multiple battery stacks in solar PV system. In: IEEE 2019 SCES Students Conference on Engineering and Systems; Allahabad, India; 2019. pp. 1-6. doi: 10.1109/SCES46477.2019.8977215

[18] Yu Y, Masumoto K, Wada K, Kado Y. A DC Power distribution system in a data center using a triple active bridge DC-DC converter. IEEJ Journal of Industry Applications 2018; 7(3): 202-209. doi: 10.1541/ieejjia.7.202

[19] Hoffmann F, Lafrenz J, Liserre M, Vazquez N. Isolated multiport converter as cost efficient solution for dc-fast charger of electric vehicle. In: IEEE 2019 IECON 45th Annual Conference of the IEEE Industrial Electronics Society; Lisbon, Portugal; 2019. pp. 4905-4910. doi: 10.1109/IECON.2019.8927087

[20] Chattopadhyay R, Gohil G, Acharya S, Nair V, Bhattacharya S. Efficiency improvement of three port high frequency transformer isolated triple active bridge converter. In: IEEE 2018 APEC Applied Power Electronics Conference and Exposition; San Antonio, TX, USA; 2018. pp. 1807-1814. doi: 10.1109/APEC.2018.8341262.